J BONE ONCOL 52 (2025) 100673

Contents lists available at ScienceDirect

Journal of Bone Oncology

journal homepage: www.elsevier.com/locate/jbo

Research Paper

A novel bone metastasis-related gene signature for predicting prognosis, anti-androgen resistance, and drug choice in prostate cancer

Yu Luo [a,1], Xiaoqi Deng [b,1], Chengcheng Wei [a,1], Zhangcheng Liu [a], Liangdong Song [a], Kun Han [a], Yunfan Li [a], Jindong Zhang [a,*], Shuai Su [a,*], Delin Wang [a,*]

[a] Department of Urology, the First Affiliated Hospital of Chongqing Medical University, Chongqing 400016, China
[b] Department of Nephrology, Zigong Fourth People's Hospital, Zigong, Sichuan Province 643000, China

HIGHLIGHTS

- Developed the BMRPS, a bone metastasis-related risk model for PCa.
- BMRPS demonstrates strong predictive ability for PCa prognosis.
- BMRPS accurately predicts prognosis in PCa with bone metastasis.
- BMRPS effectively forecasts anti-androgen resistance in PCa.
- AZD8186 shows promise as a personalized therapy linked to BMRPS in PCa.

GRAPHICAL ABSTRACT

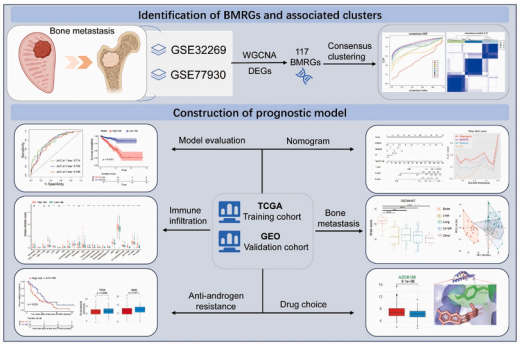

ARTICLE INFO

Keywords:
Prostate cancer
Bone metastasis
Prognostic gene signature
Anti-androgen resistance
Personalized medicine

ABSTRACT

Objective: Prostate cancer (PCa) often metastasizes to the bone, posing a significant clinical challenge. This study aims to develop a bone metastasis-related risk model for PCa.

Methods: Bone metastasis-related genes (BMRGs) were identified through a combination of differential gene expression analysis and WGCNA using GSE32269 and GSE77930 datasets. Consensus clustering analysis was employed to determine the significance of these genes in molecular subtyping of PCa. LASSO-Cox regression analysis was utilized to construct the bone metastasis-related prognostic gene signature (BMRPS). The predictive performance of BMRPS was assessed using ROC curves, Kaplan-Meier survival curves, and a predictive nomogram. The immune landscape heterogeneity of subgroups was analyzed using CIBERSORT, ESTIMATE, and xCell algorithms. Drug sensitivity and molecular docking analysis were performed to identify drugs associated with BMRPS.

Results: Forty-four BMRGs associated with the prognosis of PCa were identified. Consensus clustering revealed the pivotal role of these genes in stratifying PCa into three distinct prognostic clusters. The BMRPS, consisting of 14 BMRGs, demonstrated excellent predictive accuracy for prognosis and served as an independent prognostic factor in PCa. BMRPS effectively predicted the overall survival of bone metastatic PCa and differentiated bone metastasis from other metastatic types. BMRPS showed a close correlation with the immune landscape and

* Corresponding authors.
E-mail addresses: zhangjindong@hospital.cqmu.edu.cn (J. Zhang), sushuai930809@163.com (S. Su), wandelin@hospital.cqmu.edu.cn (D. Wang).
[1] These authors contributed equally to this work and share first authorship.

https://doi.org/10.1016/j.jbo.2025.100673
Received 27 September 2024; Received in revised form 13 January 2025; Accepted 10 March 2025
Available online 20 March 2025

immunotherapeutic response biomarkers. Additionally, BMRPS was associated with anti-androgen resistance, and AZD8186 was identified as a potential BMRPS-related drug that holds promise for personalized treatment in PCa.

Conclusion: BMRPS facilitates the prediction of prognosis and resistance to anti-androgens in PCa. It also offers insights into the molecular mechanisms of bone metastasis and aids in drug selection for the treatment of PCa.

1. Introduction

Prostate cancer (PCa) is a significant health concern affecting the male urinary system, ranking as the second leading cause of cancer-related deaths among men [1]. The standard treatments for localized PCa include surgery, radiotherapy, and active surveillance [2]. In cases of metastatic PCa, androgen deprivation therapy (ADT) plays a central therapeutic role, as androgens are crucial in driving PCa cell growth [3]. While many patients initially respond to ADT, a significant number progress to castration-resistant PCa (CRPC) due to intratumoral androgen production and aberrant activation of the androgen receptor (AR) [4,5]. CRPC is characterized by castration-level serum testosterone accompanied by biochemical recurrence (BCR) or disease progression on imaging [6]. Metastatic CRPC (mCRPC) represents the advanced stage of PCa and correlates with high mortality rate [7]. The first-line drugs for mCRPC include androgen receptor signaling inhibitors (ARSIs) such as enzalutamide and abiraterone [8]. Enzalutamide competitively inhibits androgen binding to the receptor and disrupts nuclear transport and DNA interaction [9]. Abiraterone inhibits CYP17A1, reducing androgen synthesis [10]. Inhibiting the AR signaling pathway effectively suppresses tumor growth, providing clinical benefits to patients [11,12]. However, the emergence of anti-androgen resistance poses a significant challenge [13], emphasizing the necessity for predictive indicators and a deeper understanding of the mechanisms underlying drug resistance.

PCa exhibits a notable predilection for bone metastasis, with approximately 70 % of PCa cases and up to 90 % of advanced PCa cases manifesting bone involvement [14]. PCa patients with bone metastasis typically face a median survival of under three years, with an average 5-year survival rate of merely 3 % [15]. Bone metastasis engenders severe complications such as bone disease, pathological fractures, spinal cord compression, hypercalcemia [16]. However, there is currently no specific effective treatment for bone metastasis in PCa, and the exact molecular mechanisms driving bone metastasis remain incompletely understood. In recent years, numerous studies have highlighted the pivotal role of the bone microenvironment in bone metastasis [17–19]. Interactions between cancer cells and the bone microenvironment contribute to the progression of bone metastasis [20]. Various constituents of the bone microenvironment, including mesenchymal stem cells (MSCs), bone marrow stromal cells, osteoblasts, and osteoclasts, contribute to the processes of colonization, dormancy, activation, and bone remodeling associated with bone metastasis [20]. Moreover, the bone microenvironment creates conducive conditions for the establishment of distant metastases in PCa [17]. Historically, the immunosuppressive nature of the bone metastatic microenvironment in PCa led to it being termed an "immune desert," with limited response to immune checkpoint therapy [21]. Notably, macrophage infiltration within the bone metastasis tumor microenvironment has emerged as a critical factor in tumor progression and resistance to ARSIs like enzalutamide [22]. Despite the high incidence and immense challenges posed by bone metastasis, the development of molecular predictive models specifically tailored to PCa prognosis, bone metastasis, therapeutic response remains inadequate.

In the present study, we identified a gene set related to bone metastasis and assessed their significance in PCa progression through consensus clustering analysis. Subsequently, we developed a bone metastasis-related prognostic gene signature (BMRPS) and demonstrated its robust predictive value for PCa prognosis. Furthermore, we investigated the correlation between BMRPS and bone metastasis, immune landscape, anti-androgen resistance, and drug choice in PCa. These discoveries collectively provide new perspectives on the progression, bone metastasis, and potential personalized treatment for PCa.

2. Method

2.1. Publicly available datasets

The GSE32269 and GSE77930 datasets containing primary and bone metastasis PCa samples were used to identify bone metastasis-related genes (BMRGs). The gene expression profiling of 52 normal tissues and 502 PCa tissues in the TCGA-PRAD cohort was downloaded from The Cancer Genome Atlas database (TCGA, https://portal.gdc.cancer.gov/). After data cleaning, a total of 491 PCa samples in the TCGA-PRAD cohort were included as a training cohort. The GSE21034 ($n = 140$) and GSE70770 ($n = 203$) datasets were applied as external validation cohorts. The GSE74685 and GSE66187 datasets containing samples from multiple organ metastases were used to compare the risk scores of different types of metastatic PCa samples. GSE32269, GSE77930, GSE21034, GSE70770, GSE74685 and GSE66187 datasets were downloaded from the Gene Expression Omnibus database (GEO, https://www.ncbi.nlm.nih/). In addition, SU2C dataset with mCRPC samples and clinical data on lethality was downloaded from the cBioportal database (https://www.cbioportal.org/). After excluding samples without prognostic data, a total of 73 mCRPC samples (including bone, liver, lung, and lymph node metastases) were included in this study. Additionally, after excluding missing data, the time on treatment for first-line ARSIs for 55 patients in the SU2C cohort, as reported in Abida W's study, was included in this study [23]. The expression profiles of proteins encoded by BMRPS-based genes in normal and PCa samples were downloaded from The Human Protein Atlas database (THPA, https://www.proteinatlas.org).

2.2. Differential gene expression and gene enrichment analysis

The differential gene expression analysis was performed using "Limma" R package. Significant differentially expressed genes (DEGs) between primary and bone metastatic PCa in GSE32269 and GSE77930 were considered as those with $|\log_2 \text{fold change}| \geq 1$ and p-values < 0.05. DEGs between the low- and high-risk groups of TCGA-PRAD cohort were considered as those with $|\log_2 \text{fold change}| \geq 0.7$ and p-values < 0.05. Gene Ontology (GO), Kyoto Encyclopedia of Genes and Genomes (KEGG), and Gene Set Enrichment Analysis (GSEA) were performed by the "clusterProfiler" R package. GO and KEGG analyses were conducted to identify biological processes and signaling pathways linked with DEGs. GSEA was utilized to explore the enrichment status of specific signaling pathway. We also performed comprehensive gene enrichment analysis through the Metascape database (https://metascape.org/gp) [24].

2.3. Weighted gene co-expression network analysis (WGCNA)

WGCNA was utilized to identify gene modules associated with bone metastasis based on the GSE32269 and GSE77930 using the "WGCNA" R package [25]. Initially, the top 6000 genes in GSE32269 and GSE77930, based on average gene expression, were included in the WGCNA to construct a gene co-expression network. Outlier samples were removed

based on clustering results. Subsequently, the adjacency matrix was transformed into a topological overlap matrix using an optimal soft threshold. The topological overlap matrix-based phase dissimilarity metric analysis was employed to detect gene modules, ensuring each module contained no fewer than 30 genes. Finally, correlations between modules and disease trait were established, with the module demonstrating the strongest association with bone metastasis selected as the key module for subsequent analysis.

2.4. Consensus clustering based on bone metastasis genes

The BMRGs were identified as the overlapping DEGs in the GSE32269 and GSE77930 datasets, as well as shared genes within the key modules obtained from WGCNA. Then, the BMRGs associated with DFS of PCa in the TCGA-PRAD training cohort were identified using univariate Cox regression analysis. Subsequently, these genes were then incorporated into the consensus clustering analysis using the "ConsensusClusterPlus" R package [26]. The optimal number of clusters was determined based on the cumulative distribution function (CDF) and the relative change in the area under the CDF curve. Principal Component Analysis (PCA) was employed to visualize differences in sample distributions across clusters. The Kaplan-Meier survival curves were utilized to assess variations in survival outcomes among different clusters. Additionally, single sample GSEA (ssGSEA) was performed to evaluate the differences in the activity of osteoclast-related signaling pathways (Supplementary Table 3) among the consensus clusters.

2.5. Immune landscape analysis

The infiltration abundance of immune cells and stromal cells was assessed using the CIBERSORT and xCell algorithms. Additionally, the ESTIMATE score, immune score, and stromal score of these cases were calculated using the ESTIMATE algorithm. The CIBERSORT, xCell, and ESTIMATE algorithms [27] were implemented using the "CIBERSORT," "xCell," and "estimate" R packages, respectively.

2.6. Construction and validation of prognostic gene signature

The least absolute shrinkage and selection operator (LASSO)-Cox regression analysis was employed to construct the bone metastasis-related prognostic gene signature (BMRPS). Initially, the "glmnet" R package was utilized for LASSO-Cox regression analysis, leveraging data from the TCGA-PRAD cohort. The expression levels of included genes and their corresponding weighted coefficients were then used to construct the BMRPS model using the formula: BMRPS $= \sum$ (expression of gene$_i$ $\times$ Coefficient of gene$_i$). Subsequently, the cases were stratified into low- and high-risk groups based on the median BMRPS score. Kaplan–Meier curves, generated using the "survival" and "survminer" R packages, were utilized to analyze the survival outcomes of the low- and high-risk groups. Moreover, the receiver operating characteristic (ROC) curves and the areas under the curves (AUC) were evaluated using the "pROC" and "timeROC" R packages to assess the specificity and sensitivity of the BMRPS in predicting prognosis of PCa. The same methods were performed on the GSE21034 and GSE70770 external validation cohorts.

2.7. Construction and validation of nomogram

To assess whether BMRPS serves as an independent factor for DFS of PCa, we performed univariate and multivariate Cox regression analyses. BMRPS score, age, Gleason score, pathological T stage, pathological N stage, and prostate-specific antigen (PSA) level were included as covariates. Next, we incorporated the independent predictors identified from these analyses to construct a nomogram utilizing the "rms" R package. Calibration curves were utilized to assess the consistency between actual and predicted survival outcomes, while ROC curves were employed to evaluate the specificity and sensitivity of the nomogram. Additionally, the AUC values of the nomogram and its included parameters were compared at various time points.

2.8. Genomic heterogeneity analysis

The tumor mutation burden (TMB) and microsatellite instability (MSI) of cases within the TCGA-PRAD cohort were compared between the low- and high-risk groups. Furthermore, copy number variation data were obtained from the TCGA database and analyzed using the "maftools" R package. The mutation landscape of the top 20 mutated genes was compared between the low- and high-risk groups using the "oncoplot" R package.

2.9. Drug sensitivity analysis

The drug sensitivity prediction training set, consisting of 987 cell lines and their sensitivity data to 367 compounds, was obtained from the Genomics of Drug Sensitivity in Cancer (GDSC) database (https://www.cancerrxgene.org/) [28]. Subsequently, the "oncoPredict" R package was employed to compute the drug sensitivity score of tissues in the TCGA-PRAD cohort, utilizing the information from the training set [29].

2.10. Molecular docking

The structures of the proteins encoded by BMRPS-based genes were retrieved from the AlphaFold Protein Structure Database (AlphaFold DB, https://alphafold.ebi.ac.uk) [30] and used as receptors. The structure of AZD8186 was obtained from the PubChem database (https://pubchem.ncbi.nlm.nih.gov/) and used as a ligand. AutoDock software (version 1.5.7) was used to accomplish the removal of water molecules, hydrogenation, prediction of docking sites for core targets, and molecular docking [31]. Finally, the optimal binding energy of the top 10 core components was visualized by PyMOL (version 2.5.3) [32].

2.11. Statistical analysis

Statistical analysis was conducted using R software (version 4.3.1) and GraphPad Prism (version 8.0.2). The "psych" R package was utilized to calculate correlation coefficients and assess statistical significance. Kaplan-Meier survival analysis employed the log-rank test. For two-group comparisons, the *t*-test was employed for continuous variables, whereas the chi-squared test was applied for categorical variables in three-group comparisons. A p-value less than 0.05 was considered statistically significant.

3. Results

3.1. Identification of BMRGs

The workflow chart of this study was shown in Fig. 1. We identified 220 up-regulated and 313 down-regulated DEGs between bone metastatic PCa samples and primary PCa samples in GSE32269, and 2214 up-regulated and 1511 down-regulated genes in GSE77930 (Fig. 2A). According to the Venn tool, GSE32269 and GSE77930 shared 72 up-regulated DEGs and 23 down-regulated DEGs (Fig. 2B). Next, we performed WGCNA to identify hub gene module associated with bone metastasis. Following the original sample outlier test, 49 samples in GSE32269 and 40 samples in GSE77930 were included in WGCNA, respectively (Fig. S1A). After selecting the optimal soft threshold, a total of 11 and 7 modules were identified in GSE32269 and GSE77930, respectively (Fig. S1B and S1C). The correlation between the modules and disease trait was then examined (Fig. 2C and 2D). The turquoise module in GSE32269 ($R = 0.83$, $P < 0.0001$) and the yellow module in GSE77930 ($R = 0.89$, $P < 0.0001$) with the highest correlation coefficient were chosen as the key modules. The 714 genes in the turquoise

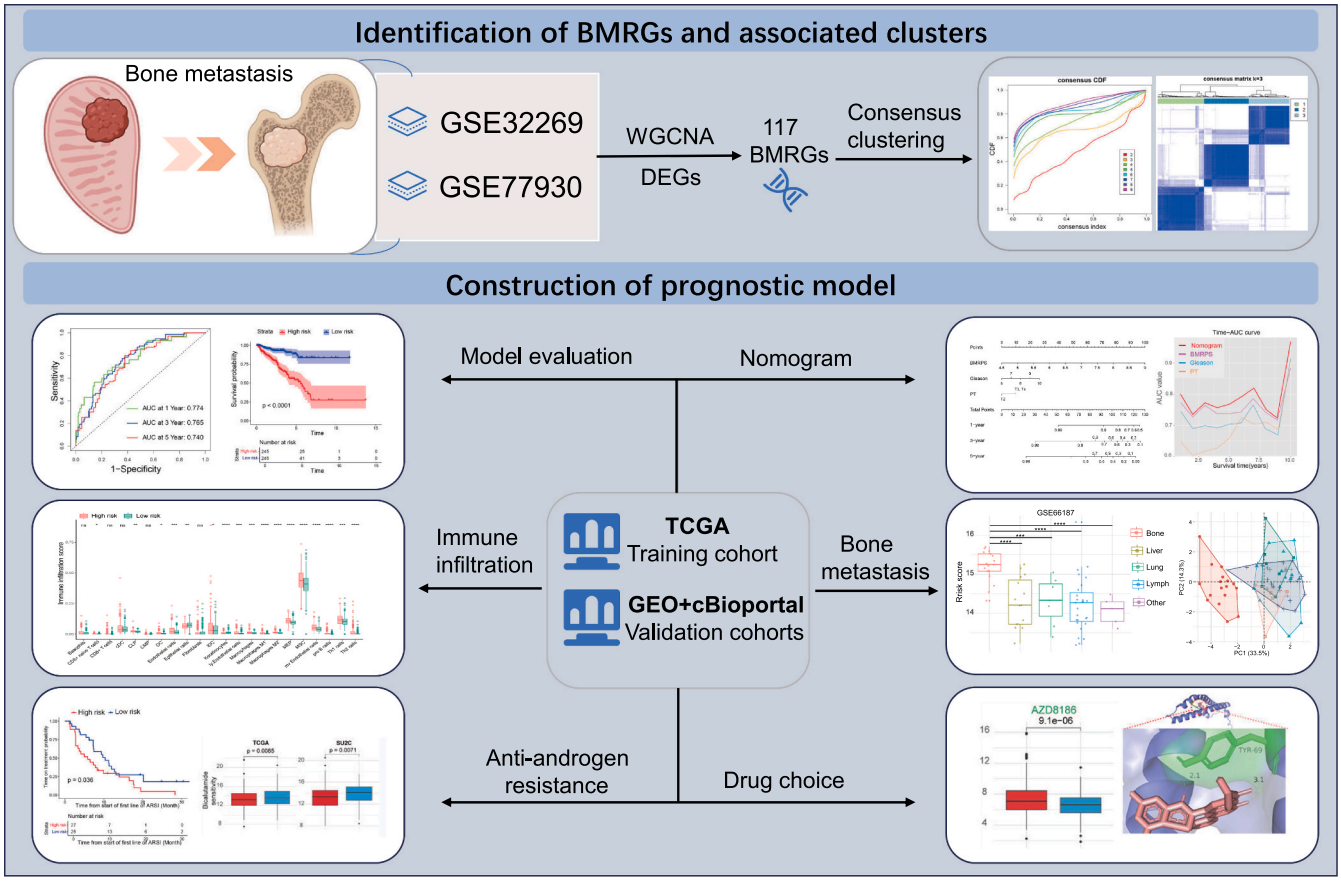

Fig. 1. The work flow chart of this study.

module and 417 genes in the yellow module exhibited strong correlations not only within their corresponding modules but also with bone metastasis (Fig. 2E and 2F). Subsequently, 22 shared genes were identified between the two key modules (Fig. 2G), which did not overlap with the shared DEGs of GSE32269 and GSE77930. Therefore, a total of 117 genes were recognized as bone metastasis-related genes (BMRGs) (Supplementary Table 1). Importantly, GO enrichment analysis revealed the association of these genes with "extracellular matrix organization", "ossification", "neutrophil degranulation", "neutrophil activation involved in the immune response", and "response to mechanical stimulus" (Fig. 2H). Additionally, KEGG enrichment analysis indicated their involvement in "ECM-receptor interaction", "cholesterol metabolism", "Focal adhesion", and "osteoclast differentiation" (Fig. 2I). These findings highlight the critical role of BMRGs in the process of bone metastasis, and these genes potentially impact the advancement of bone metastasis through the regulation of extracellular matrix remodeling.

3.2. Identification of BMRGs-related clusters

Among the 117 BMRGs, 44 were associated with the disease-free survival (DFS) of PCa according to the univariate Cox regression analysis (Supplementary Table 2). We then performed consensus clustering analysis to further identify the significance of these genes in molecular subtyping of PCa. Based on the CDF and the relative change of the area under the CDF curve, the TCGA-PRAD cohort was successfully stratified into three clusters by the 44 BMRGs (Fig. 3A-3C). Cluster 1 comprises 173 cases of PCa, Cluster 2 comprises 166 cases, and Cluster 3 comprises 152 cases. The result of Principal Component Analysis (PCA) indicated a distinct distribution of the three clusters, suggesting different expression patterns of these 44 genes among the three clusters (Fig. 3D). Importantly, the result of Kaplan–Meier survival analysis demonstrated a significant difference in DFS among the three clusters, with Cluster 1 having the best prognosis and Cluster 3 having the worst (Fig. 3E). Further analysis revealed that the cluster with a poorer prognosis had a higher proportion of patients with higher Gleason score (Fig. 3G), advanced pathological T stage (Fig. 3H), advanced pathological N stage (Fig. 3I), and disease progression or recurrence (Fig. 3J). We further compared the differences in the immune landscape among the three clusters based on ESTIMATE algorithm, revealing significant disparities in immune score, stromal score, and ESTIMATE score (Fig. 3F). Immune infiltration analysis revealed that the cluster with a poorer prognosis was accompanied by a higher abundance of M2 macrophages and lower abundance of plasma cells and resting mast cells (Fig. 3K). Furthermore, GSEA indicated that "chemokine signaling pathway," "cytokine-cytokine receptor interaction," "leukocyte transendothelial migration," and "osteoclast differentiation" signaling pathway were activated in the combined Clusters 2 and 3 compared to Cluster 1 (Fig. 3L). Further ssGSEA revealed that osteoclast-related signaling pathways were significantly enriched in the combined Clusters 2 and 3 compared to Cluster 1 (Fig. S1D), suggesting that these consensus clusters may have a higher predisposition to bone metastasis [33]. Collectively, these results further demonstrate the crucial roles of the 44 BMRGs in the progression and bone metastasis of PCa.

3.3. Construction and validation of BMRPS

LASSO-Cox regression analysis was then performed based on the expression of the 44 BMRGs in the TCGA-PRAD cohort, resulting in the selection of 14 genes: COL11A1, HNRNPAB, STAB1, ADORA3, OLFML3, CDCA3, AIDA, MYH11, KBTBD11, MT1E, MRPL33, EFR3A, ACYP1, and LMNB2, to construct the BMRPS (Fig. 4A and 4B). In the TCGA-PRAD cohort, HNRNPAB, CDCA3, KBTBD11, ACYP1, and LMNB2 were

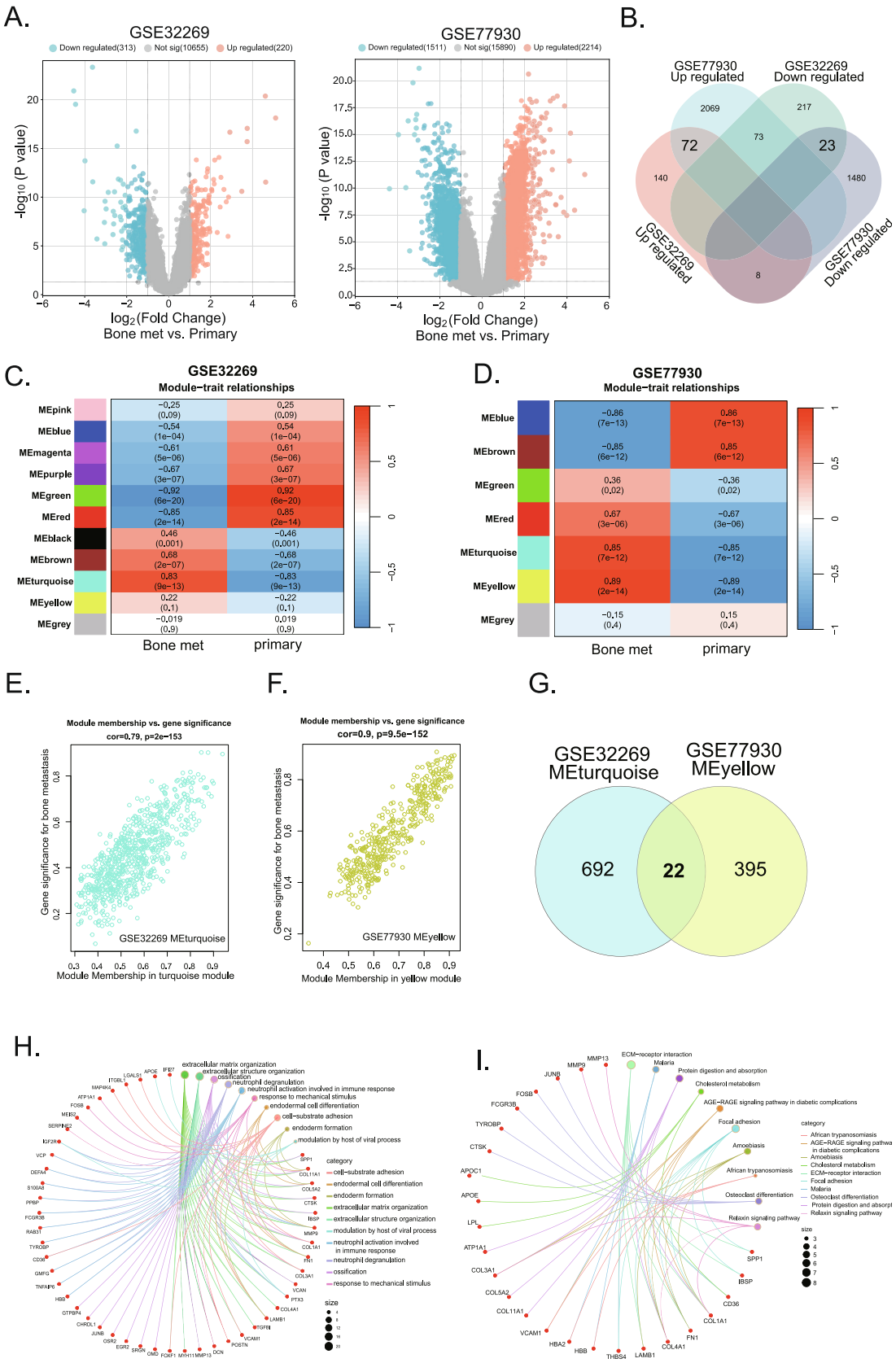

Fig. 2. Identification of BMRGs. (A) The volcano plots illustrate the DEGs in GSE32269 and GSE77930. (B) Venn diagram illustrates the shared up-regulated and down-regulated genes of GSE32269 and GSE77930. (C) and (D) Heatmaps depict the correlation between module eigengenes and bone metastasis. (E) and (F) Scatter plots of module eigengenes in the key modules of GSE32269 (E) and GSE77930 (F). (G) Venn diagram illustrates the shared genes of key modules in GSE32269 and GSE77930. (H) The top 10 biology processes associated with the BMRGs in the results of GO enrichment analysis. (I) The top 10 pathways of KEGG enrichment analysis for the BMRGs.

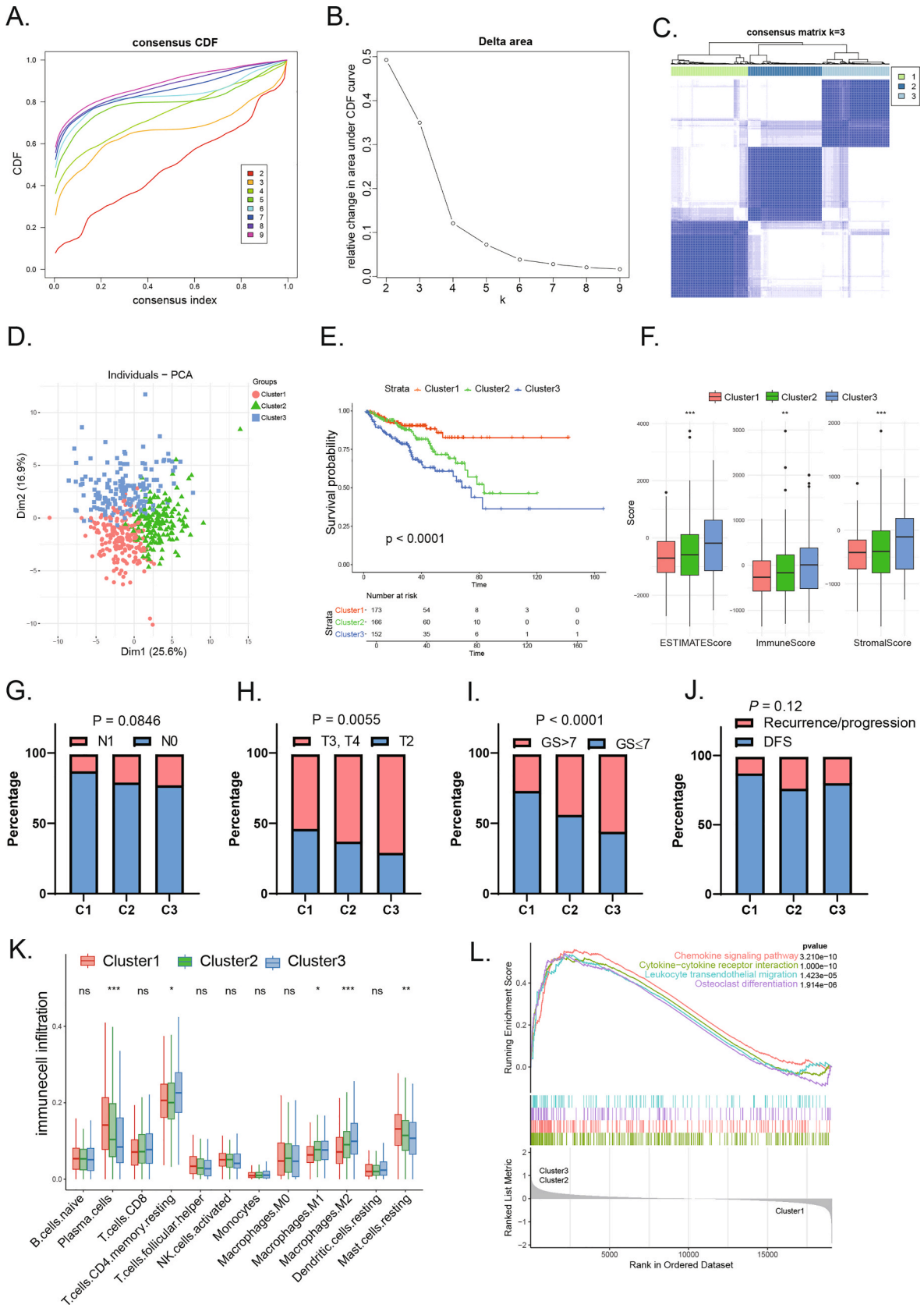

Fig. 3. Identification of BMRGs-related clusters. (A) CDF curves of different k values in the consensus clustering analysis. (B) Relative change in area under CDF curves according to different k values. (C) The consensus clustering of 44 BMRGs in the three clusters. (D) PCA plot illustrating the distribution among the three clusters. (E) Kaplan–Meier survival analysis for the three clusters. (F) Differences of tumor microenvironment scores among the three clusters according to ESTIMATE algorithm. (G–J) Differences in clinicopathological features among the three clusters. (K) Differences in immune cells infiltration among the three clusters based on CIBERSORT algorithm. (L) GSEA for illustrating signaling pathway. *, $P < 0.05$; **, $P < 0.01$; ***, $P < 0.001$; ns, not significant.

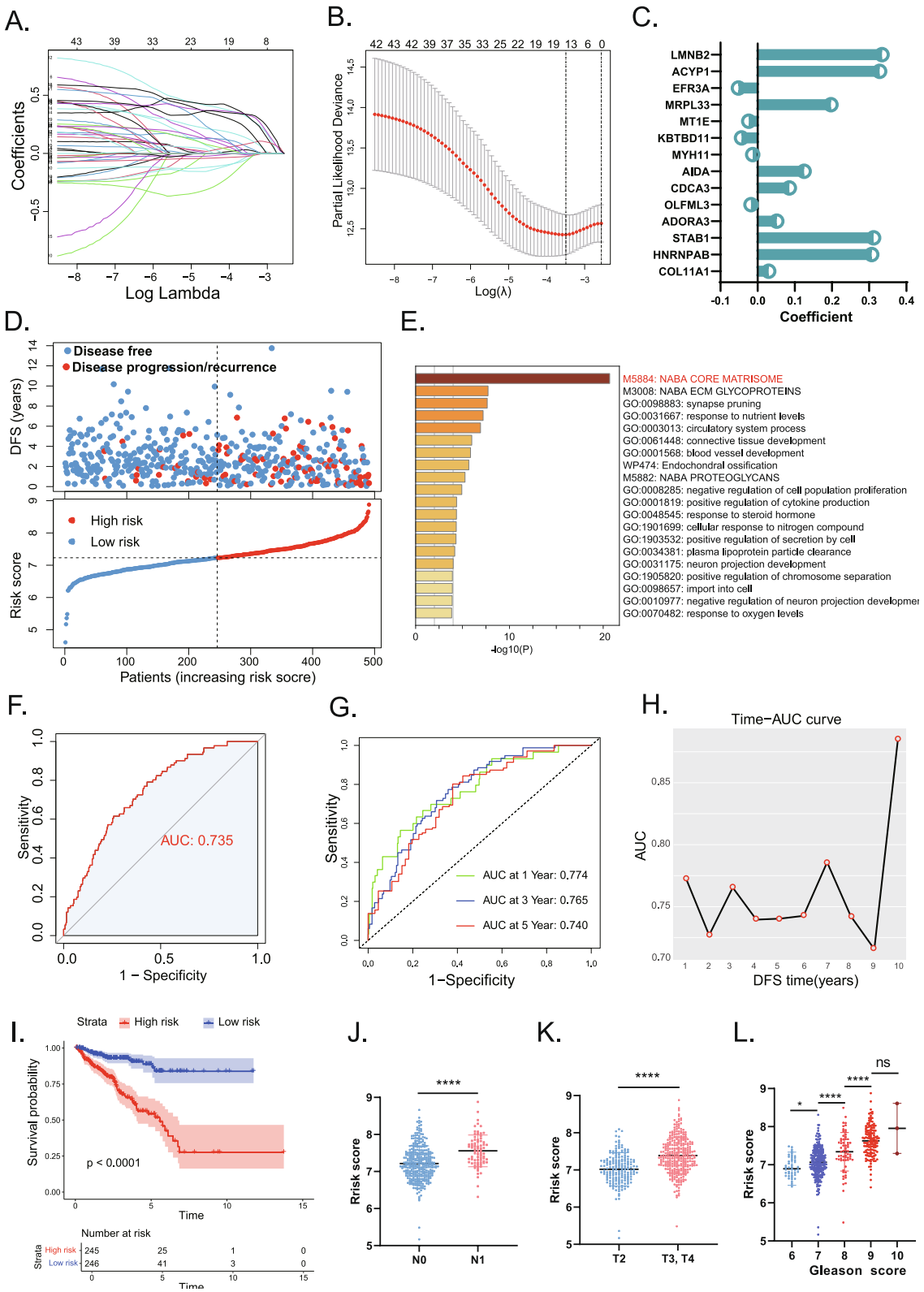

Fig. 4. Construction and validation of BMRPS. (A) The LASSO coefficient profiles of different quantitative variables. (B) Ten-fold cross-validation for the selection of tuning parameter (λ). (C) The BMRPS constructed by 14 BMRGs and corresponding coefficients. (D) DFS statuses of patients in the TCGA-PRAD cohort according to increasing BMRPS score. (E) Gene enrichment analysis of DEGs between the low- and high-risk groups of the TCGA-PRAD cohort. (F-H) ROC curve (F), time-dependent ROC curves (G) and time-dependent AUC curve (H) for evaluating the sensitivity and specificity of BMRPS in predicting DFS. (I) Kaplan–Meier survival analysis for the low- and high-risk groups of the TCGA-PRAD cohort. (J–L) The association of BMRPS with clinicopathologic features including pathological N stage (J), pathological T stage (K), and Gleason score (L). *, $P < 0.05$; ****, $P < 0.0001$; ns, not significant.

found to be up-regulated in the PCa compared to the normal prostate, and OLFML3, AIDA, MYH11, MT1E, and EFR3A were found to be down-regulated (Supplementary Fig. 2A). Additionally, the protein expression profiles in the THPA database revealed higher expression of HNRNPAB, LMNB2, and ACYP1, and lower expression of AIDA, MYH11, MT1E, and EFR3A in PCa compared to normal prostate tissue (Supplementary Fig. 3B). Subsequently, the gene expression of the 14 BMRGs and their LASSO-Cox coefficients and were extracted to construct the bone metastasis-related prognostic gene signature (BMRPS) based on the TCGA-PRAD cohort according to the following formula: BMRPS = COL11A1 × 0.030 + HNRNPAB × 0.307 + STAB1 × 0.312 + ADORA3 × 0.051 + OLFML3 × (−0.018) + CDCA3 × 0.085 + AIDA × 0.125 + MYH11 × (−0.013) + KBTBD11 × (−0.043) + MT1E × (−0.024) + MRPL33 × 0.197 + EFR3A × (−0.052) + ACYP1 × 0.328 + LMNB2 × 0.335 (Fig. 4C). The TCGA-PRAD cohort was then stratified into low- and high- risk group based on the medium BMRPS score. The high-risk group demonstrated a higher proportion of disease progression or recurrence and shorter DFS time compared to the low-risk group, in

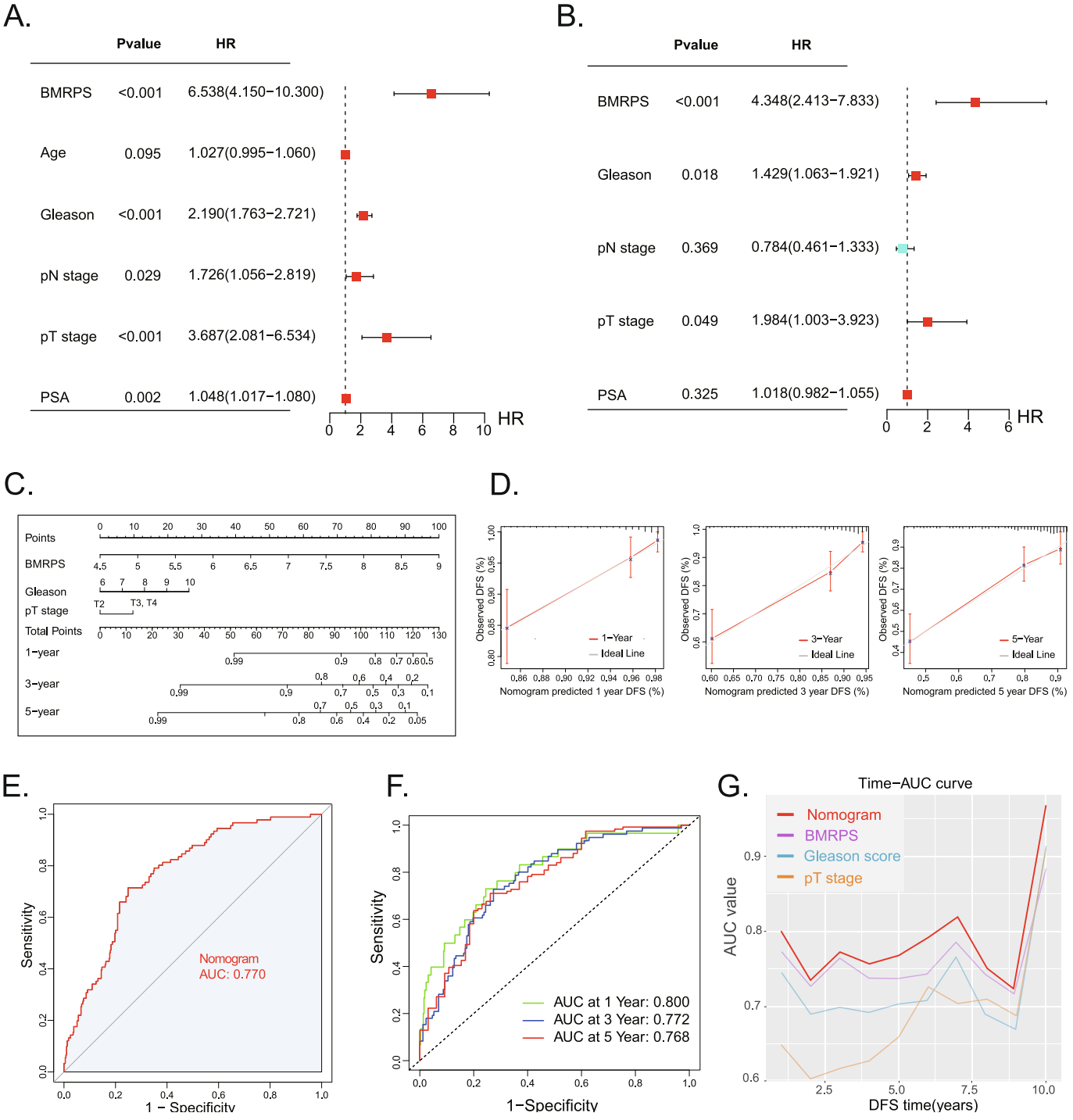

Fig. 5. Construction and validation of nomogram. (A) and (B) Forest plots of univariate (A) and multivariate (B) Cox regression analysis. (C) A prognostic nomogram based on BMRPS, Gleason score, and pathological T stage. (D) Calibration curves for evaluating the accuracy of the nomogram. (E) and (F) ROC curves (E) and time-dependent ROC curves (F) of the nomogram for predicting DFS. (G) Time-dependent AUC curves of the nomogram, BMRPS, Gleason score, and pathological T stage for predicting DFS.

accordance with the increasing risk score (Fig. 4D and Supplementary Fig. 2C). Importantly, ROC curve showed an AUC of 0.735 (Fig. 4F), and the time-dependent ROC curves indicated the AUC at 1, 3, and 5 years were 0.774, 0.765, and 0.74 for BMRPS in predicting DFS, respectively (Fig. 4G), indicating excellent sensitivity and specificity. We further plotted a curve of AUC values over time, where AUC values remain consistently above 0.7 over 1 to 10 years (Fig. 4H), indicating excellent stability of BMRPS. Then, Kaplan–Meier survival curves revealed a significantly worse prognosis for the high-risk group compared to the low-risk group ($P < 0.0001$) (Fig. 4I). Further analysis revealed that BMRPS score was associated with N stage (Fig. 4J), T stage (Fig. 4K), and Gleason score (Fig. 4L). The applicability of BMRPS was comprehensively assessed using GSE21034 and GSE70770 external validation cohorts, demonstrating good performance (Supplementary Fig. 3A–3H). Furthermore, the DEGs between the low- and high- risk groups were closely correlated with "NABA CORE MATRISOME" (Fig. 4E), which is an ensemble of genes encoding core extracellular matrix. This association offers molecular mechanistic insights into the elevated risk associated with BMRPS. Taken together, these results demonstrated the valuable predictive efficiency in assessing the prognosis of PCa.

3.4. Construction and validation of nomogram

To identified whether BMRPS is an independent risk parameter of DFS in PCa, we performed univariate Cox and multivariate Cox regression analysis in TCGA-PRAD cohort. Univariate Cox analysis revealed that BMRPS, Gleason score, T stage, N stage, and PSA level were associated with DFS of PCa (Fig. 5A). Multivariate Cox regression analysis identified BMRPS, Gleason score, and T stage as independent prognostic parameters of DFS in PCa (Fig. 5B). Subsequently, we included these three factors to construct a nomogram, as shown in Fig. 5C. Calibration curves were then constructed to assess the nomogram's accuracy,

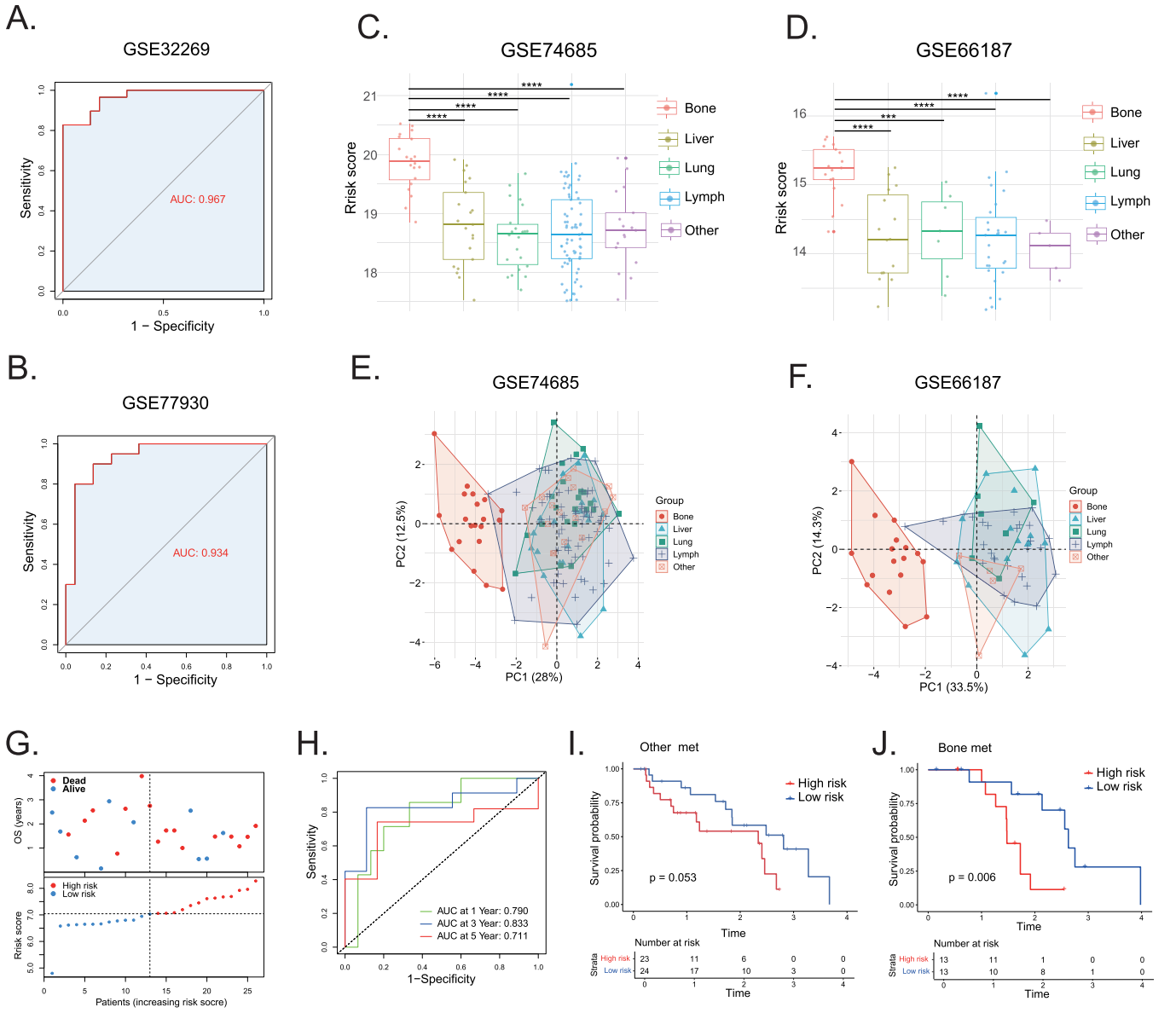

Fig. 6. BMRPS is correlated with the prognosis of patients with bone metastasis. (A) and (B) ROC curves of BMRPS for distinguishing primary and bone metastatic PCa in GSE32269 (A) and GSE77930 (B). (C) and (D) Comparison of the BMRPS scores of bone metastasis and other organ metastases in GSE74685 and GSE66187. (E) and (F) PCA analysis for GSE74685 and GSE66187 based on the expression profiles of BMRPS-based genes. (G) OS statuses of bone metastatic PCa in the SU2C cohort based on increasing BMRPS score. (H) Time-dependent ROC curves for BMRPS in predicting the OS of bone metastatic PCa. (I) and (J) Kaplan–Meier survival analysis for the low- and high-risk groups in bone metastatic PCa (J) and other metastatic cases combined (liver, lung, and lymph node) (I). ***, $P < 0.001$; ****, $P < 0.0001$.

demonstrating a good fit between predicted probabilities of 1-, 3-, and 5-year DFS and observed survival rates (Fig. 5D). The ROC curve for the nomogram showed an AUC of 0.770 in predicting DFS (Fig. 5E). The time-dependent ROC curves indicated AUC values of 0.8, 0.772, and 0.768 at 1, 3, and 5 years, respectively (Fig. 5F). Additionally, we compared AUC values over time for the nomogram, BMRPS, Gleason score, and T stage, revealing consistently higher AUC values for the nomogram compared to BMRPS, Gleason score, and T stage over 1 to 10 years (Fig. 5G). These results collectively showcase the outstanding predictive capability and long-term reliability of the predictive nomogram.

3.5. BMRPS is correlated with the prognosis of patients with bone metastasis

We next explored the association of BMRPS with bone metastasis. First, we conducted ROC curve using the BMRPS risk score to differentiate between sample types (primary and bone metastatic). The results indicated that the BMRPS score exhibited excellent discriminative ability, with AUC values of 0.967 and 0.934 in the GSE32269 and GSE79930 datasets, respectively (Fig. 6A and 6B). This demonstrates that BMRPS has strong predictive performance in distinguishing normal tissues from bone metastatic tumors. Furthermore, we compared BMRPS scores among multiple organ metastases of PCa in GSE74685 and GSE66187 datasets. Interestingly, the BMRPS score was significantly higher in bone metastatic tissues compared to liver, lung, lymph node, and other soft tissue metastases (Fig. 6C and 6D). The distribution of bone metastasis samples in the PCA space is notably distinct from that of other metastatic tissues, showing clear spatial separation (Fig. 6E and 6F). These results indicate that the expression patterns of BMRPS-based gene in bone metastases differ significantly from those in other types of metastatic tissues, suggesting a strong association between altered BMRPS-based gene expression and bone metastasis. Then, we explored the association of BMRPS with the prognosis of patients with bone metastasis in the SU2C dataset. As shown in Fig. 6G, higher proportion of deaths and shorter overall survival (OS) time in the high-risk group were observed compared to the low-risk group. In addition, the time-dependent ROC curves for BMRPS in predicting OS revealed AUCs of 0.79, 0.833, and 0.711 at 1, 3, and 5 years, respectively (Fig. 6H). Interestingly, Kaplan–Meier survival analysis indicated that a higher BMRPS score was associated with OS of bone metastasis (Fig. 5J), but not in other metastatic cases combined (liver, lung, and lymph node metastases) (Fig. 5I). Taken together, these findings suggest that BMRPS-based genes may play a critical role in the process of bone metastasis, and BMRPS could serve as a valuable indicator for predicting the prognosis of PCa with bone metastasis.

3.6. The association of BMRPS with immune landscape and immunotherapeutic biomarkers

Bone metastasis is closely linked to immune-related processes [20], and bone metastasis tumor microenvironment has been reported to be immunosuppressive [34]. Therefore, we explored the relationship between BMRPS and the immune landscape of PCa. As depicted in Fig. 7A, BMRPS showed significant correlation with immune score, stroma score, and ESTIMATE score in PCa. Further analysis revealed that the high-risk group exhibited higher infiltration levels of immunosuppressive cells including macrophages, endothelial cells, and MSCs compared to the low-risk group (Fig. 7B). Additionally, the high-risk group showed significantly higher expression of immune checkpoint genes, such as CTLA4, CD276, and PDCD1, compared to the low-risk group (Fig. 7C). Moreover, the high-risk group demonstrated significantly higher tumor mutation burden (TMB) (Fig. 7D) and microsatellite instability (MSI) (Fig. 7E) compared to the low-risk group. Furthermore, oncoplots revealed that the top 20 mutated genes were more frequently mutated in the high-risk group, with notable prominence observed in genes such as TP53, SPOP, TTN, and KMT2D (Fig. 7F). These findings collectively suggest that BMRPS is associated with immunosuppressive and multiple biomarkers of immunotherapeutic response, indicating its potential as a valuable indicator for immunotherapy.

3.7. BMRPS is associated with anti-androgen resistance

Macrophage is the key stroma cell type significantly enriched in bone-metastatic PCa compared with primary tumor and metastases in other organs. Besides, macrophage promoted anti-androgen resistance in bone metastasis by regulating ECM-receptor interaction of PCa cells [22]. In our study, we observed a significant increase in macrophage infiltration in the high-risk group (Fig. 7B), and BMRPS exhibited a significantly positive correlation with macrophage infiltration (Fig. 8A–C). Besides this, BMRPs was highly related to "NABA_CORE_MATRISOME" (Fig. 4E). The androgen response signaling pathway was found to be suppressed in the high-risk group in the TCGA-PRAD cohort (Fig. 8D). These prompted us to explore the association between BMRPS and anti-androgen resistance in PCa. Analyzing data from 55 patients treated with first-line androgen receptor signaling inhibitors (ARSIs) in the SU2C dataset, we stratified the patients into low- and high-risk groups based on their median BMRPS scores. A higher rate of drug withdrawal (indicating resistance) [22] and a shorter duration of ARSIs treatment were observed in the high-risk group compared to the low-risk group (Fig. 8E). The time-dependent ROC curves for predicting ARSIs resistance displayed AUC values of 0.706, 0.742, and 0.749 at 6, 18, and 24 months, respectively (Fig. 8F), with AUC values almost consistently exceeding 0.7 within 30 months (Fig. 8G). Furthermore, the high-risk group exhibited a shorter duration of ARSIs treatment than the low-risk group, suggesting an increased likelihood of developing resistance to ARSIs among these patients (Fig. 8H). For further substantiation, we compared the drug sensitivity of bicalutamide (one of ARSIs) between high-risk and low-risk groups in the TCGA and SU2C cohorts. The results indicate that regardless of whether it is primary PCa in the TCGA-PRAD cohort or mCRPC in the SU2C cohort, the high-risk group exhibit significantly lower sensitivity to bicalutamide compared to the low-risk group (Fig. 8I). Besides this, BMRPS was negatively correlated with bicalutamide sensitivity both in TCGA-PRAD ($R = -0.15$, $P = 0.000819$) and SU2C cohorts ($R = -0.38$, $P < 0.0001$) (Fig. 8J and 8K). Collectively, these findings underscore BMRPS as a reliable predictor for anti-androgen resistance.

3.8. Identification of AZD8186 as a potential drug associated with BMRPS

To explore the value of BMRPS in personalized and precision treatment of PCa, we compared the drug sensitivity of the low- and high-risk groups in the TCGA-PRAD cohort to 10 anti-PCa drugs previously reported [35,36]. Compared to the low-risk group, the high-risk group exhibited lower sensitivity to most of these drugs, but exhibited higher sensitivity to AZD8186 (Fig. 9A). Furthermore, BMRPS showed positive correlation with the sensitivity of AZD8186 ($R = 0.24$, $P < 0.0001$) (Fig. 9B). We therefore further evaluated the affinity of AZD8186 to the proteins encoded by the BMRPS-based genes using molecular docking analysis. The results revealed that AZD8186 could form stable hydrogen bonds with these proteins, with a minimum binding energy of less than −5 kcal/mol in 13 out of 14 conformations (Fig. 9C), indicating a high degree of stability in the interaction between AZD8186 and the proteins encoded by BMRPS-based genes. The top 10 conformations with the lowest binding energies based on hydrogen bonding are illustrated in Fig. 9D. Taken together, these findings suggest that AZD8186 could be considered as an alternative treatment option associated with BMRPS.

4. Discussion

Bone metastasis remains a significant clinical challenge due to its

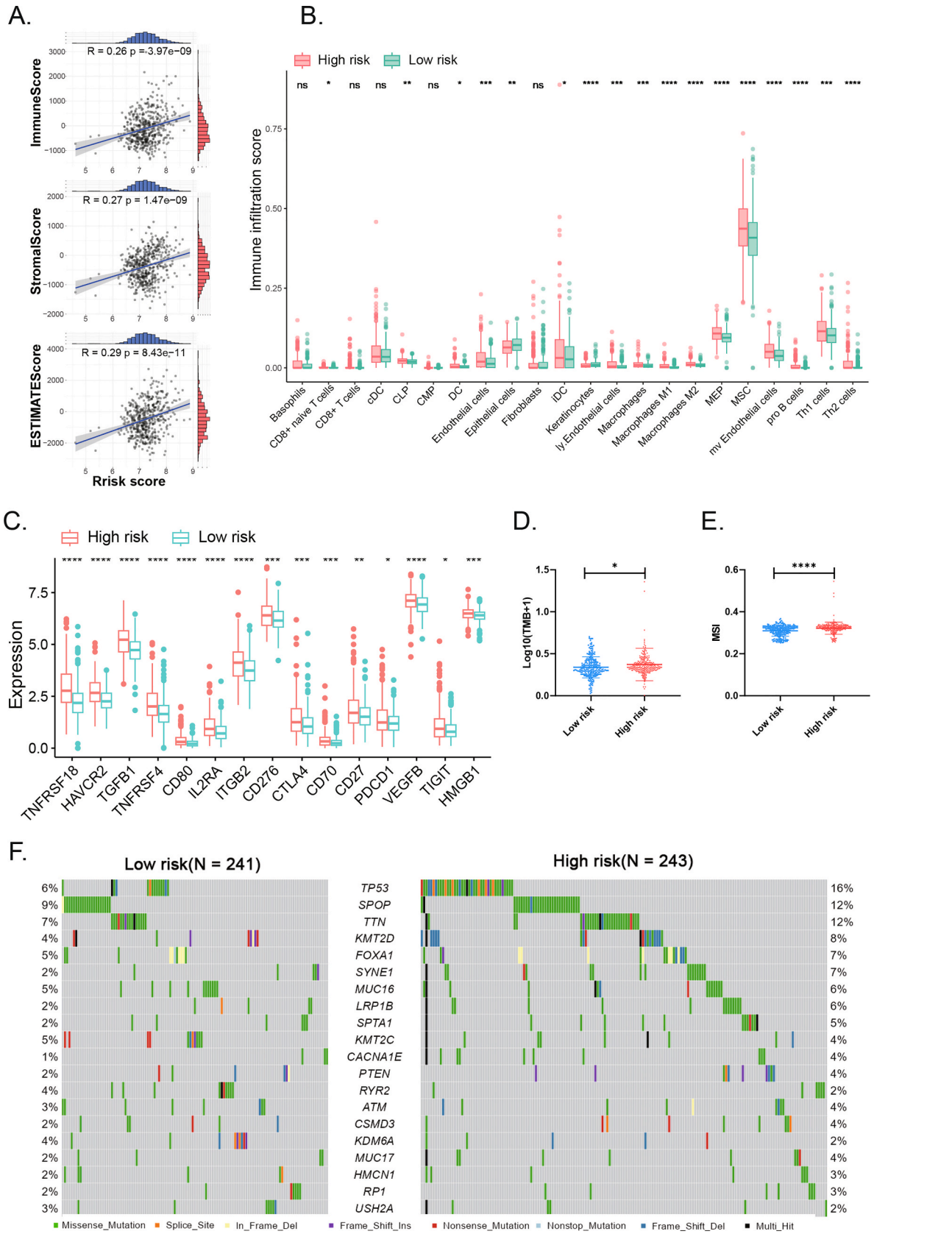

Fig. 7. The association of BMRPS with immune landscape and immunotherapeutic biomarkers. (A) Correlations of BMRPS with immune score, stromal score and ESTIMATE score. (B) The box plots illustrating the differences in immune cell and stromal cell infiltration levels between the low- and high-risk groups of TCGA-PRAD cohort based on xCell algorithm. (C) Comparing the expression of immune checkpoint genes between the high- and low-risk groups of TCGA-PRAD cohort. (D) and (E) Comparing TMB and MSI between the high- and low-risk groups of TCGA-PRAD cohort. (F) The oncoplots of the top 20 mutated genes in the high-and low-risk groups. *, $P < 0.05$; **, $P < 0.01$; ***, $P < 0.001$; ****, $P < 0.0001$; ns, not significant.

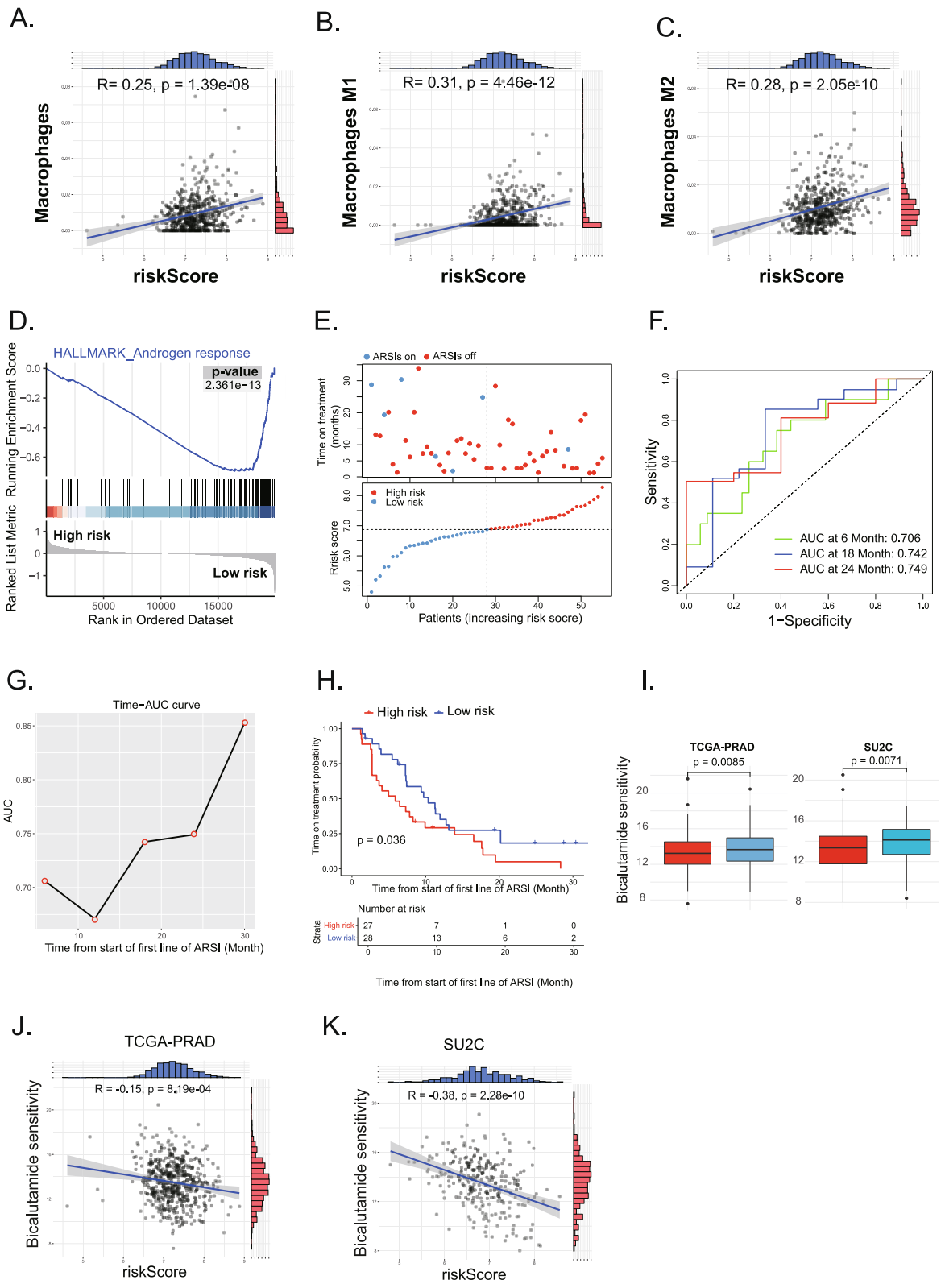

Fig. 8. BMRPS is associated with anti-androgen resistance. (A)–(C) Scatter plots showing the correlation between BMRPS and the infiltration of macrophage (A), M1 macrophage (B), and M2 macropahge (C). (D) GSEA for the androgen response signaling pathways in the TCGA-PRAD cohort. (E) ARSIs treatment status of mCRPC in the SU2C cohort based on increasing BMRPS score. (F) Time-dependent ROC curves for BMRPS in predicting ARSIs resistance. (G) Time-dependent AUC curve of BMRPS in predicting ARSIs resistance within 30 months. (H) Kaplan–Meier analysis for time on treatment (indicating resistance) probability of mCRPC. (I) The drug sensitivity of the low- and high-risk groups in the TCGA-PRAD and SU2C cohorts to bicalutamide. (J) and (K) Correlations of BMRPS with the sensitivity score of bicalutamide in the TCGA-PRAD and SU2C cohorts.

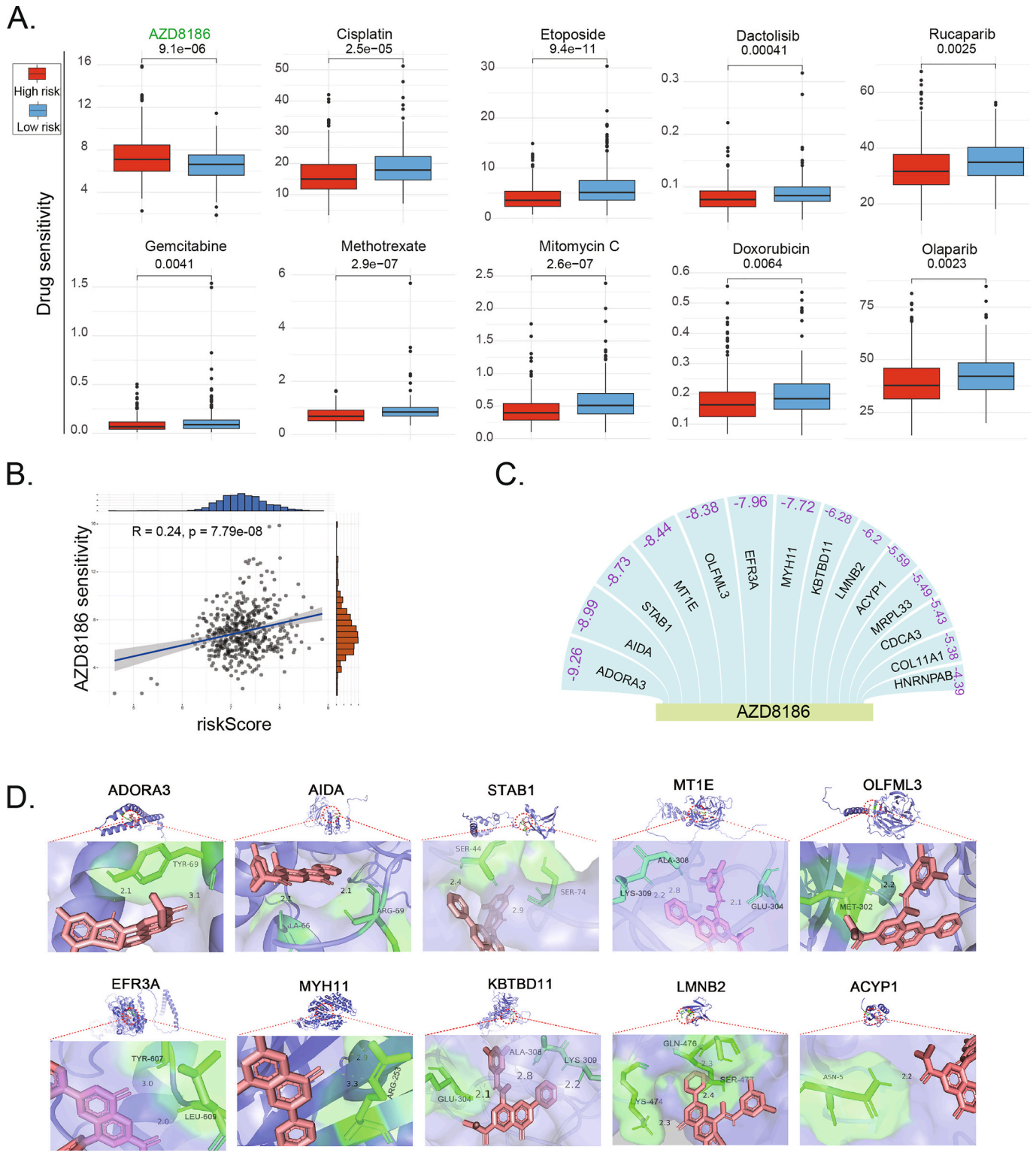

Fig. 9. Identification of AZD8186 as a potential drug associated with BMRPS. (A) Box plots showing the sensitivity score of the low- and high-risk groups of TCGA-PRAD cohort to 10 anti-PCa drugs previously reported. (B) Scatter plots showing the correlation between BMRPS and the sensitivity score of AZD8186 in the TCGA-PRAD cohort. (C) The minimum binding energies of the optimal conformation of the docking between AZD8186 and the proteins encoded by the BMRPS-based genes. (D) Conformations of AZD8186 binding to proteins encoded by BMRPS-based genes via hydrogen bonding. The top 10 conformations with the lowest binding energies were shown.

intricate interplay with the tumor microenvironment and its resistance to conventional treatments [37]. Unraveling the molecular intricacies of bone metastasis holds promise for developing targeted therapies that could potentially improve patient outcomes and quality of life. The high propensity of PCa for bone metastasis motivated the development of the BMRPS based on BMRGs, which demonstrates excellent predictive value and stability in forecasting prognosis of PCa with bone metastasis. BMRPS shows close correlation with bone metastasis tissue and serves as

a reliable indicator for prognosis of patients with bone metastasis. Therefore, our study provides valuable insights into the molecular mechanisms driving PCa dissemination to bone.

In this study, the BMRGs were enriched in "extracellular matrix organization," "extracellular structure organization," "ECM-receptor interaction," and the increased BMRPS risk was closely associated with "NABA CORE MATRISOME". As an important component of both the tumor and bone microenvironments, extracellular matrix is linked to numerous cellular processes in tumor cells, including cell adhesion, differentiation, migration, and angiogenesis [38], and it provides substantial support for the colonization of bone metastatic tumor cells [39]. To date, several studies have demonstrated a connection between ECM remodeling and bone metastasis in PCa. For example, PCa cells with bone metastatic potential exhibit a propensity to diminish their adhesion to the ECM, facilitating their entry into the bloodstream or lymphatic circulation. This process culminates in their homing to the bone marrow, where they establish secondary tumors [40,41]. Moreover, as pivotal bone cells involved in bone remodeling, osteoclasts and osteoblasts contribute to ECM remodeling and the vicious cycle of bone metastasis [38,42]. PCa cells disrupt the balance between bone resorption by osteoclasts and bone formation by osteoblasts, fueling tumor progression within the bone microenvironment [43]. Therefore, elevated BMRPS risk may be associated with the remodeling of the extracellular matrix, potentially increasing the likelihood of bone metastasis. The BMRPS-based genes are expected to become special therapeutic targets in the progression of bone metastasis in PCa.

The loss of PTEN has been associated with the progression and poor clinical outcomes of PCa [44]. Increased PI3K signaling resulting from PTEN loss is implicated in the development of various solid tumors, including PCa [45]. AZD8186, a potent and selective PI3Kβ inhibitor, has been extensively studied in PCa. In preclinical models of PTEN-negative PCa, AZD8186 combined with ADT has demonstrated high efficacy [46]. Furthermore, combining AZD8186 with ARSIs, docetaxel, and the mTOR inhibitor vistusertib has shown increased antitumor activity in an additive manner in PTEN-negative PCa [36,47,48]. Importantly, AZD8186 exhibited acceptable safety and tolerability in solid tumors, including PCa, and its combination with abiraterone acetate/prednisone was well tolerated [36]. In our study, a high BMRPS score indicated increased sensitivity to AZD8186 in PCa, and AZD8186 demonstrated consistent binding to proteins encoded by BMRPS-based gens through hydrogen bonding. Based on existing research findings, we hypothesize that AZD8186 may inhibit the progression of bone metastasis and the development of anti-androgen resistance in PCa by targeting the expression of BMRPS-based genes.

While our findings are promising, several limitations should be noted. First, both the training and validation datasets used in constructing our model were obtained from existing public databases, potentially introducing inherent biases from these data sources. In addition, due to the limitations of microarray data, some important BMRGs may have been overlooked. Moreover, further prospective cohorts and original experiments are necessary to confirm the relationship between BMRPS and bone metastasis incidence or skeletal-related events. Finally, the widespread application of BMRPS relies on the broader adoption of bone biopsy in clinical practice. Although bone biopsy has not yet been widely implemented, recent technological advancements have demonstrated the feasibility and broad applicability of combining bone biopsy with next-generation sequencing [49,50]. Therefore, we believe that BMRPS has the potential to become a valuable tool with the continuous development of these technologies.

CRediT authorship contribution statement

Yu Luo: Writing – review & editing, Writing – original draft, Methodology, Data curation, Conceptualization. **Xiaoqi Deng:** Writing – review & editing, Methodology, Conceptualization. **Chengcheng Wei:** Writing – review & editing, Methodology, Formal analysis, Conceptualization. **Zhangcheng Liu:** Writing – review & editing, Software, Methodology. **Liangdong Song:** Visualization, Validation, Methodology. **Kun Han:** Writing – original draft, Validation. **Yunfan Li:** Validation, Software. **Jindong Zhang:** Writing – review & editing, Project administration, Funding acquisition. **Shuai Su:** Writing – review & editing, Project administration, Investigation, Data curation. **Delin Wang:** Writing – review & editing, Supervision, Project administration, Investigation, Funding acquisition, Conceptualization.

Funding

This work was supported by grants from the Doctoral program of the first affiliated hospital of Chongqing Medical University (CYYY-BSYJSCXXM-202332, CYYY-BSYJSKYCXXM202421) and Chongqing Natural Science Foundation project (CSTB2024NSCQ-MSX0317).

Declaration of competing interest

The authors declare that they have no known competing financial interests or personal relationships that could have appeared to influence the work reported in this paper.

Acknowledgements

We express our gratitude for the abundant data generously provided by public databases for this study. The availability of these public databases has significantly contributed to advancing our research endeavors, facilitating comprehensive analysis and interpretation of the data. We also acknowledge the support from the Doctoral Program of the First Affiliated Hospital of Chongqing Medical University and the Chongqing Natural Science Foundation Project.

Appendix A. Supplementary data

Supplementary data to this article can be found online at https://doi.org/10.1016/j.jbo.2025.100673.

References

[1] O. Bergengren, et al., 2022 update on prostate cancer epidemiology and risk factors-a systematic review, Eur. Urol. 84 (2) (2023) 191–206.
[2] K. Desai, J.M. McManus, N. Sharifi, Hormonal therapy for prostate cancer, Endocr. Rev. 42 (3) (2021) 354–373.
[3] D.E.N. C, et al., Androgen deprivation therapy and cardiovascular risk in prostate cancer, Minerva Urol. Nephrol. 74(5) (2022) 508–517.
[4] Z. Zhu, et al., Loss of dihydrotestosterone-inactivation activity promotes prostate cancer castration resistance detectable by functional imaging, J. Biol. Chem. 293 (46) (2018) 17829–17837.
[5] L. Zhou, et al., ACSS3 represses prostate cancer progression through downregulating lipid droplet-associated protein PLIN3, Theranostics 11 (2) (2021) 841–860.
[6] H.I. Scher, et al., Design and end points of clinical trials for patients with progressive prostate cancer and castrate levels of testosterone: recommendations of the Prostate Cancer Clinical Trials Working Group, J. Clin. Oncol. 26 (7) (2008) 1148–1159.
[7] J. Sturge, M.P. Caley, J. Waxman, Bone metastasis in prostate cancer: emerging therapeutic strategies, Nat. Rev. Clin. Oncol. 8 (6) (2011) 357–368.
[8] T. Yanagisawa, et al., Androgen receptor signaling inhibitors in addition to docetaxel with androgen deprivation therapy for metastatic hormone-sensitive prostate cancer: a systematic review and meta-analysis, Eur. Urol. 82 (6) (2022) 584–598.
[9] X. Chen, et al., Drug resistance of enzalutamide in CRPC, Curr. Drug Targets 19 (6) (2018) 613–620.
[10] J. Malikova, et al., CYP17A1 inhibitor abiraterone, an anti-prostate cancer drug, also inhibits the 21-hydroxylase activity of CYP21A2, J. Steroid Biochem. Mol. Biol. 174 (2017) 192–200.
[11] A.J. Armstrong, et al., ARCHES: a randomized, phase III study of androgen deprivation therapy with enzalutamide or placebo in men with metastatic hormone-sensitive prostate cancer, J. Clin. Oncol. 37 (32) (2019) 2974–2986.
[12] K. Fizazi, et al., Abiraterone acetate plus prednisone in patients with newly diagnosed high-risk metastatic castration-sensitive prostate cancer (LATITUDE): final overall survival analysis of a randomised, double-blind, phase 3 trial, Lancet Oncol. 20 (5) (2019) 686–700.

[13] S.A.J. Buck, et al., Cross-resistance and drug sequence in prostate cancer, Drug Resist. Updat. 56 (2021) 100761.
[14] Y. Kfoury, et al., Human prostate cancer bone metastases have an actionable immunosuppressive microenvironment, Cancer Cell 39 (11) (2021), 1464–1478 e8.
[15] F. Zhao, et al., Sites of synchronous distant metastases and prognosis in prostate cancer patients with bone metastases at initial diagnosis: a population-based study of 16,643 patients, Clin. Transl. Med. 8 (1) (2019) 30.
[16] S. Tsukamoto, et al., Current overview of treatment for metastatic bone disease, Curr. Oncol. 28 (5) (2021) 3347–3372.
[17] W.J. Zhang, et al., The bone microenvironment invigorates metastatic seeds for further dissemination, Cell 184 (9) (2021), 2471-+.
[18] S. Li, Y. Kang, Y. Zeng, Targeting tumor and bone microenvironment: Novel therapeutic opportunities for castration-resistant prostate cancer patients with bone metastasis, Biochim. Biophys. Acta 1879 (1) (2024) 189033.
[19] X. Lin, et al., The bone extracellular matrix in bone formation and regeneration, Front. Pharmacol. 11 (2020).
[20] X.Y. Zhang, Interactions between cancer cells and bone microenvironment promote bone metastasis in prostate cancer, Cancer Commun. 39 (1) (2019).
[21] C. Palena, J.L. Gulley, A rare insight into the immunosuppressive landscape of prostate cancer bone metastases, Cancer Cell 39 (11) (2021) 1450–1452.
[22] X.F. Li, et al., Macrophages promote anti-androgen resistance in prostate cancer bone disease, J. Exp. Med. 220 (4) (2023).
[23] W. Abida, et al., Genomic correlates of clinical outcome in advanced prostate cancer, PNAS 116 (23) (2019) 11428–11436.
[24] Y. Zhou, et al., Metascape provides a biologist-oriented resource for the analysis of systems-level datasets, Nat. Commun. 10 (1) (2019) 1523.
[25] X. Deng, et al., Identification of GMFG as a novel biomarker in IgA nephropathy based on comprehensive bioinformatics analysis, Heliyon 10 (7) (2024) e28997.
[26] M.D. Wilkerson, D.N. Hayes, ConsensusClusterPlus: a class discovery tool with confidence assessments and item tracking, Bioinformatics 26 (12) (2010) 1572–1573.
[27] K. Zhu, et al., Development and validation of a novel lipid metabolism-related gene prognostic signature and candidate drugs for patients with bladder cancer, Lipids Health Dis. 20 (1) (2021) 146.
[28] W. Yang, et al., Genomics of Drug Sensitivity in Cancer (GDSC): a resource for therapeutic biomarker discovery in cancer cells, Nucl. Acids Res. 41 (Database issue) (2013) D955–D961.
[29] D. Maeser, R.F. Gruener, R.S. Huang, oncoPredict: an R package for predicting in vivo or cancer patient drug response and biomarkers from cell line screening data, Brief. Bioinform. 22 (6) (2021).
[30] M. Varadi, et al., AlphaFold Protein Structure Database: massively expanding the structural coverage of protein-sequence space with high-accuracy models, Nucl. Acids Res. 50 (D1) (2022) D439–D444.
[31] O. Trott, A.J. Olson, AutoDock Vina: improving the speed and accuracy of docking with a new scoring function, efficient optimization, and multithreading, J. Comput. Chem. 31 (2) (2010) 455–461.
[32] D. Seeliger, B.L. de Groot, Ligand docking and binding site analysis with PyMOL and Autodock/Vina, J. Comput. Aided Mol. Des. 24 (5) (2010) 417–422.
[33] C. Chen, et al., Icariin inhibits prostate cancer bone metastasis and destruction via suppressing TAM/CCL5-mediated osteoclastogenesis, Phytomedicine 120 (2023) 155076.
[34] C. Yin, et al., BHLHE22 drives the immunosuppressive bone tumor microenvironment and associated bone metastasis in prostate cancer, J. Immunother. Cancer 11 (3) (2023).
[35] W. Zhu, et al., Multi-omics analysis reveals a macrophage-related marker gene signature for prognostic prediction, immune landscape, genomic heterogeneity, and drug choices in prostate cancer, Front. Immunol. 14 (2023) 1122670.
[36] A.D. Choudhury, et al., A phase I study investigating AZD8186, a potent and selective inhibitor of PI3Kbeta/delta, in patients with advanced solid tumors, Clin. Cancer Res. 28 (11) (2022) 2257–2269.
[37] A. Hosseini, et al., Role of the bone marrow microenvironment in drug resistance of hematological malignances, Curr. Med. Chem. 29 (13) (2022) 2290–2305.
[38] A.I. Alford, K.M. Kozloff, K.D. Hankenson, Extracellular matrix networks in bone remodeling, Int. J. Biochem. Cell Biol. 65 (2015) 20–31.
[39] J.N. Kang, et al., Tumor microenvironment mechanisms and bone metastatic disease progression of prostate cancer, Cancer Lett. 530 (2022) 156–169.
[40] R.B. Berish, et al., Translational models of prostate cancer bone metastasis, Nat. Rev. Urol. 15 (7) (2018) 403–421.
[41] B.J. Grindel, et al., Matrilysin/MMP-7 cleavage of perlecan/HSPG2 complexed with semaphorin 3A supports FAK-mediated stromal invasion by prostate cancer cells, Sci. Rep. 8 (1) (2018) 7262.
[42] L.M. Cook, et al., Integrating new discoveries into the “vicious cycle” paradigm of prostate to bone metastases (vol 33, pg 511, 2014), Cancer Metastasis Rev. 33 (4) (2014) 1125.
[43] J.B. Wu, et al., MAOA-dependent activation of Shh-IL6-RANKL signaling network promotes prostate cancer metastasis by engaging tumor-stromal cell interactions, Cancer Cell 31 (3) (2017) 368–382.
[44] S. Schwartz, et al., Feedback Suppression of PI3Kα Signaling in-mutated tumors is relieved by selective inhibition of PI3Kβ, Cancer Cell 27 (1) (2015) 109–122.
[45] L. Salmena, A. Carracedo, P.P. Pandolfi, Tenets of PTEN tumor suppression, Cell 133 (3) (2008) 403–414.
[46] R.B. Marques, et al., High efficacy of combination therapy using PI3K/AKT inhibitors with androgen deprivation in prostate cancer preclinical models, Eur. Urol. 67 (6) (2015) 1177–1185.
[47] U. Hancox, et al., Inhibition of PI3Kbeta signaling with AZD8186 inhibits growth of PTEN-deficient breast and prostate tumors alone and in combination with docetaxel, Mol. Cancer Ther. 14 (1) (2015) 48–58.
[48] J.T. Lynch, et al., Combined inhibition of PI3Kbeta and mTOR inhibits growth of PTEN-null tumors, Mol. Cancer Ther. 17 (11) (2018) 2309–2319.
[49] R. Donners, et al., Multiparametric bone MRI targeting aides lesion selection for CT-guided sclerotic bone biopsies in metastatic castrate resistant prostate cancer, Cancer Imaging 23 (1) (2023) 121.
[50] V. Sailer, et al., Bone biopsy protocol for advanced prostate cancer in the era of precision medicine, Cancer 124 (5) (2018) 1008–1015.